Comparison of pulmonary arterial flow phenomena in spiral and Lecompte models by computational fluid dynamics

Tongdar Tang, PhD[a]
Ing-Sh Chiu, MD, PhD, MDiv[b]
Hsin-Chi Chen, PhD[c]
Koung-Yo Cheng, BS[b]
Shyh-Jye Chen, MD[d]

Objectives: The transposed great arteries are simply reversed by means of a conventional arterial switch operation with the Lecompte maneuver without resumption of their spiral relationship. We seek to clarify the functional implications of the spiral relationship of the great arteries by means of mathematic modeling.

Methods: Computational fluid dynamics is used to compare flow phenomena of the spiral and Lecompte (nonspiral) models under various body surface areas.

Results: The velocity profile and wall-shear stress distribution are more uniform for the spiral than for the Lecompte model. The pressure drop and power loss ratio are smaller for the spiral than the Lecompte model for all the body surface areas investigated. The power loss ratio increases abruptly starting from 0.43 m^2 of body surface area for the Lecompte model. At that specific stage, after arterial switch operation with the Lecompte maneuver, suprapulmonary stenoses occur most frequently.

Conclusions: Reconstructing the great arteries in spiral fashion might be recommended because the blood flow patterns are more streamlined than those of the Lecompte maneuver. Initiation of stenosis might be minimized to some extent.

From the Department of Mechanical Engineering, Huafan University,[a] the Department of Mechanical Engineering, Chungyuan University,[c] and the Departments of Surgery[b] and Medical Imaging,[d] National Taiwan University Hospital, Taipei, Taiwan.

Received for publication Sept 28, 2000; revisions requested Jan 17, 2001; revisions received Jan 24, 2001; accepted for publication Feb 20, 2001.

Address for reprints: Ing-Sh Chiu, MD, PhD, Department of Surgery, National Taiwan University Hospital, No. 7 Chung-Shan S Rd, Taipei, Taiwan 100 (E-mail: ingsh@ha.mc.ntu.edu.tw).

J Thorac Cardiovasc Surg 2001;122:529-34

0022-5223/2001 $35.00 + 0 **12/1/115230**

doi:10.1067/mtc.2001.115230

The arterial switch operation (ASO) has become the procedure of choice for transposition of the great arteries (TGA).[1,2] TGA is considered to be an anteroposterior reversal of the great arteries.[3,4] Nonexistence of the normal spiral relationship in TGA has not been widely appreciated. The posterior pulmonary bifurcation is mobilized anteriorly to the aorta (so-called Lecompte maneuver)[5] in an effort simply to reverse the transposed great arteries. The functional implications of spirally related great arteries remain unknown, and their spiral relationship is usually not resumed in TGA. The fluid dynamic phenomena and energetic differences between the spiral and Lecompte (nonspiral) models of the great arteries may be small. However, small differences may have significant implications for the long-term follow-up. It is widely known that suprapulmonary stenosis remains a significant problem, with a peak incidence at 9 months after conventional ASO.[6,7] Nonetheless, the Lecompte maneuver is used in almost all cases except some posterior or side-by-side transpositions.[8,9] Although there might be no pressure gradient across this anterior and upward tilting region initially, the flow inside the preaortic pulmonary pathway is not streamlined. The cross section of the pulmonary trunk (PT) becomes oval after the Lecompte maneuver.[10] It is circular, provided that the compression from the posterior aorta is not present as a result of spiral recon-

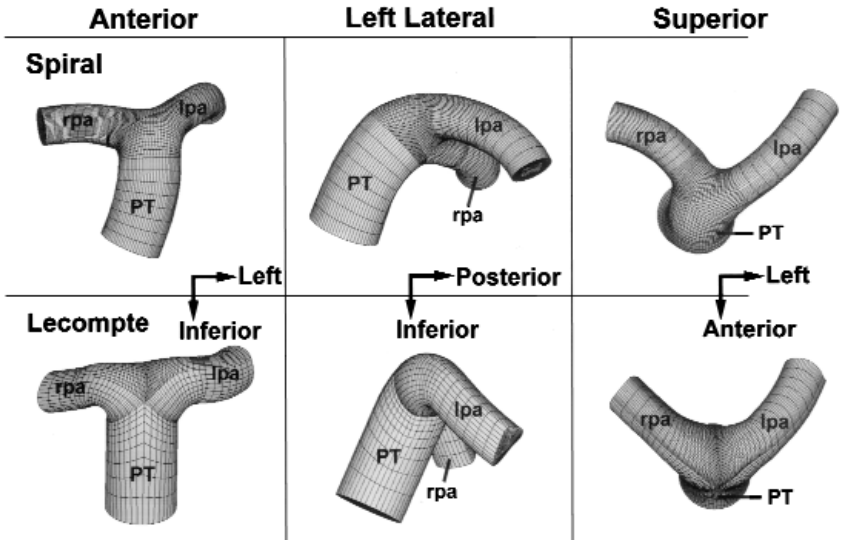

Figure 1. Computational meshes of 3-dimensional spiral *(upper panel)* and Lecompte *(lower panel)* models viewed from anterior, left lateral, and superior aspects. The anterior and left lateral views are the normal views of the angiogram. In the superior view the undepicted aorta is in front of the RPA and right lateral to the PT for the spiral model, whereas it is encircled behind the PT and between the RPA and LPA for the Lecompte model.

struction, as created naturally. We therefore advocate resumption of the normal spiral relationship of the great arteries in TGA.[11]

In contrast to the suprapulmonary stenosis, supra-aortic stenosis is rare after ASO with the Lecompte maneuver.[7] To clarify the functional implications of spiral relationship of the great arteries, we established the pulmonary component in the spiral and Lecompte models of the great arteries by means of computer-aided engineering. Computational fluid dynamics based on the finite volume method are used to compute the flow field. From the calculated velocity and pressure data, energy loss and wall-shear stress are estimated, compared, and evaluated.

CHD

Methods

Description of Geometric Models

The geometries of 2 prototypical models including the PT, right pulmonary artery (RPA), and left pulmonary artery (LPA) are modeled on a computer on the basis of the general contours that were seen on electron beam–computed tomograms from 21 patients after 2 types of neonatal ASO: 10 underwent the conventional ASO with the Lecompte maneuver,[5] and 11 underwent the spiral reconstruction.[11] The surface contours of these models, spiral and Lecompte, are created by the computer-aided design software IDEAS (SDRC Co, Milford, Ohio) and transferred to the computer-aided engineering software ANSYS (ANSYS, Inc, Canonsburg, Pa). The prototypical computational models of hexahedral meshes are then generated (Figure 1).

So that the flow phenomena of these 2 models could be compared under various body surface areas (BSAs), Table 1 lists the derived models' diameters, flow rates, and mean velocities of PT according to the following empiric equations:

$$\text{Flow rate } (Q_{PT}\ [\text{L/min}]) = 2.4 \times \text{BSA } (\text{m}^2) \quad (1)$$

$$\text{Diameter of PT } (D_{PT}\ [\text{mm}]) = 3.1831 \times (3.5869 \times \log[\text{BSA}(\text{cm}^2)] - 9.5431) \quad (2)[12]$$

$$\text{Mean velocity at the PT } (V_{PT}\ [\text{cm/s}]) = 1666 \times \frac{Q_{PT}\ (\text{L/min})}{\pi D_{PT}(\text{mm})^2/4} \quad (3)$$

The coefficient 1666 exists because of unit conversion. The dimensions of these 3-dimensional models are assumed to vary proportionally to the diameter of the PT (D_{PT}). The shape of the derived models remains the same as that of the prototype model. For each model, the diameters of RPA and LPA outlets are both specified to be $1/\sqrt{2}$ times D_{PT}. The total outlet area is therefore the same as the PT's entrance area ($\pi D_{PT}^2/4$).

Calculations of Velocity and Pressure Field by Computational Fluid Dynamics

The computational mesh data are exported into a CFD solver STAR-CD (Computational Fluid Dynamics Corp, Ltd, London, United Kingdom), and flow calculations are performed. The flow is considered to be steady, laminar, Newtonian, and incompressible. The governing equations are 3-dimensional continuity and momentum (Navier-Stokes) equations.[13] The viscosity of blood (μ) is set at 0.003 kg $\cdot$ m^{-1} $\cdot$ s^{-1}, with a density (ρ) of 1060 kg/m^3.

The computational domain is divided into discrete control volumes (cells). The total cell number of each model is approximate-

TABLE 1. The simulated conditions for the spiral and Lecompte models

BSA (m^2)	0.25	0.30	0.35	0.39	0.40	0.43	0.45	0.50	0.55	0.65	0.75	0.95	1.15	1.35	1.95
Q_{PT} (L/min)	0.60	0.72	0.84	0.94	0.96	1.03	1.08	1.20	1.32	1.56	1.80	2.28	2.76	3.24	3.72
D_{PT} (mm)	8.42	9.32	10.09	10.62	10.75	11.11	11.33	11.86	12.33	13.16	13.87	15.04	15.99	16.78	17.47
V_{PT} (cm/s)	17.96	17.58	17.52	17.60	17.63	17.75	17.84	18.12	18.43	19.12	19.86	21.39	22.92	24.41	25.88

D_{PT}, Diameter of the PT; Q_{PT}, flow rate; V_{PT}, mean velocity at the PT.

ly 48,000. The governing equations are discretized by the finite volume method. The Semi-Implicit Method for Pressure-Linked Equations algorithm is implemented for the calculations. The algebraic equation sets are solved by means of iterative practice. A linear upwind differentiation scheme is implemented.

Boundary Conditions

A uniform flow velocity is used at the PT entrance as the inlet boundary condition. Pure outlet boundary ($\frac{\partial \vec{V}}{\partial \vec{n}} = 0$) is used at the exits of the RPA and LPA, where $\vec{V}$ is the velocity vector and $\vec{n}$ is the outward unit normal vector. The flow ratio between the RPA and LPA is specified to be 1.50% of the PT flow rates (through the RPA and LPA, respectively. At the vessel wall, no-slip boundary condition ($\vec{V} = 0$) is applied. A fixed reference pressure is specified at the PT entrance.

Wall-Shear Stress Estimation

Wall-shear stress is estimated from the near-wall velocity data and correlated with stenotic lesion distribution. Wall-shear stress (τ_S) is defined as follows:

$$\tau_S = \mu\left(\frac{\partial V_z}{} + \frac{\partial V_r}{}\right) \quad (4)$$

Where τ_S is the wall-shear stress, V_z is the axial velocity component near the wall, V_r is the radial velocity component near the wall, z is the axial direction, and r is the radial distance from the wall.

Power Loss Ratio

To investigate the geometric effects in flow energy loss, dissipated power (W_{diss}) and power loss ratio (C_e) are computed according to the velocity and pressure data at the PT entrance and RPA and LPA outlets. Dissipated power and power loss ratio are defined as follows[14]:

$$W_{diss} = (\tfrac{1}{2}\rho V_{PT}^2 + P_{PT})Q_{PT} - (\tfrac{1}{2}\rho V_{RPA}^2 + P_{RPA})Q_{RPA} - (\tfrac{1}{2}\rho V_{LPA}^2 + P_{LPA})Q_{LPA} \quad (5)$$

and

$$C_e = \frac{W_{diss}}{(\tfrac{1}{2}\rho V_{PT}^2 + P_{PT})Q_{PT}} \quad (6)$$

where V_{PT}, V_{RPA}, and V_{LPA} are the space-averaged velocities at the PT entrance, RPA outlet, and LPA outlet, respectively. P_{PT}, P_{RPA}, and P_{LPA} are the space-averaged pressure values at the PT entrance, RPA outlet, and LPA outlet, respectively. Q_{PT}, Q_{RPA}, and Q_{LPA} are the total flow rates at the PT entrance, RPA outlet, and LPA outlet, respectively. It should be noted that the total power at the PT entrance is identical for both models when the same BSA is specified because of the identical conditions of inlet pressure, total flow rate, and uniform inlet velocity.

Results

The velocity vector and pressure contour plots at the midplane of the spiral and Lecompte models at 0.43 m^2 of BSA are shown in Figures 2 and 3, respectively.

Velocities

The near wall geometry changes smoothly, and neither vortices nor separation regions are observed in either model (Figure 2). As the flow moves toward distal sites of the branching pulmonary arteries, velocity acceleration becomes apparent. The velocity acceleration occurs at the initial branching sites from the PT into the LPA and RPA of the Lecompte model, whereas velocity is accelerating more uniformly in the branches of the spiral model. The velocity distribution is less uniform for the Lecompte than for the spiral model. Strong flow disturbance resulting from the sharp turning angles from the PT to the RPA and LPA is evident. Profile shifting toward the superior surface, which is attributed to the centrifugal force induced by the curvature of the branching arteries, is notable in the RPA of the spiral model. High wall-shear stress is therefore expected to occur at the superior surface. A comparison of the velocity contours of both models indicates that the velocity field is more in streamline for the spiral model.

Pressure

The presented pressure data are values relative to the fixed reference pressure at the PT inlet (Figure 3). In both models smooth pressure gradient is noted, and the stagnation point near the flow divider of the bifurcation has the highest pressure. The stagnation point represents the location of motion of free blood particles and low wall-shear stress that is prone to initiate a pathologic lesion. The adverse pressure gradient, which is the common cause of flow separation and vortex, does not exist in either model. When the pressure changes between the inlets and outlets of both models are compared, the pressure drop of the Lecompte model is higher than that of the spiral model, suggesting that the spiral model possesses smoother flow field than the Lecompte model. Pressure energy loss for the Lecompte model is considered substantial. In addition, pressure gradient and pressure drop are higher in the RPA than in the LPA of the Lecompte model.

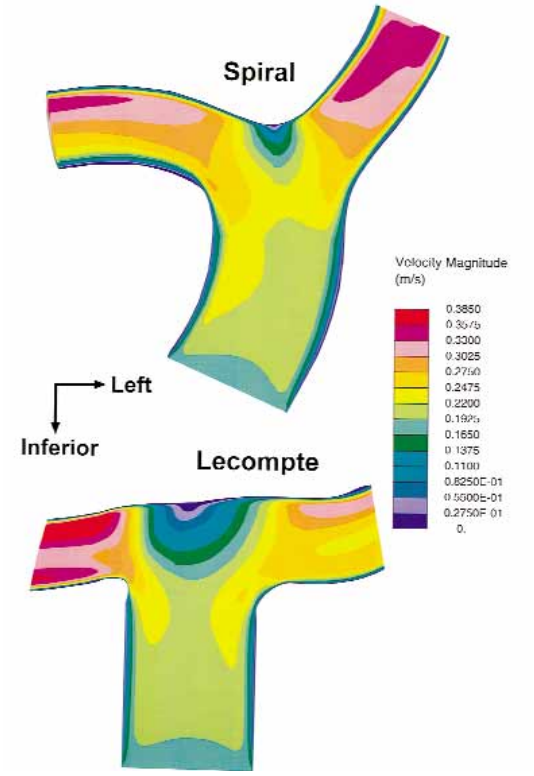

Figure 2. The midplane velocity contour plots of 2 models viewed from the anterior aspect at 0.43 m^2 of BSA. Compared with the spiral model, velocity is less uniform for the Lecompte model because maximum velocity regions *(red zone)* exist near the RPA outlet, and a large minimum velocity region *(blue zone)* is located at the flow divider of the bifurcation. Significant velocity acceleration is more apparent at the initial branching sites of the PT into RPA and LPA for the Lecompte model, whereas smoother velocity transition is shown for the spiral model. Flow disturbance is estimated to be higher for the Lecompte model than that of the spiral model.

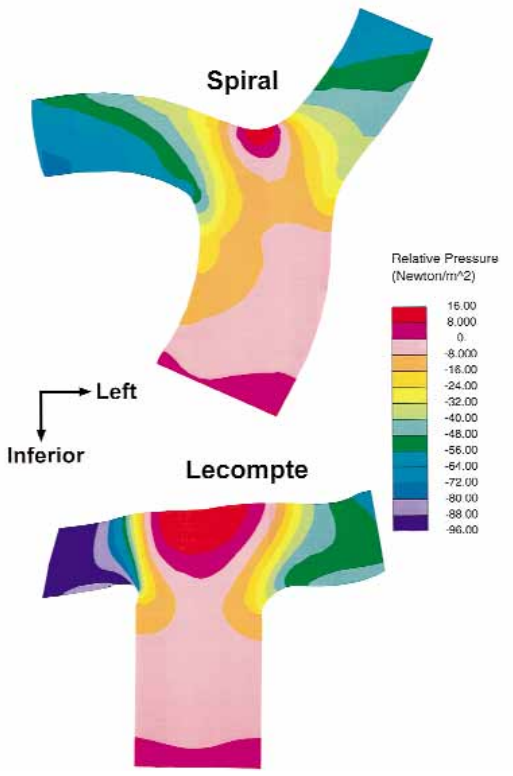

Figure 3. The midplane pressure contour plots of 2 models viewed from the anterior aspect at 0.43 m^2 of BSA. The pressure data presented are values with respect to the fixed reference pressure at the PT inlet. In both models smooth pressure gradient is noted, and the stagnation point near the flow divider of the bifurcation has the highest pressure. The pressure drop between the PT inlet and the model outlets is smaller for the spiral than for the Lecompte model, suggesting that the spiral model possesses a smoother flow field than the Lecompte model. Thus, pressure energy loss for the Lecompte model is substantial. *Red zone*, Maximum velocity magnitude; *blue zone*, minimum velocity magnitude.

CHD

Wall-Shear Stress

The wall-shear stress data under steady flow conditions of different BSAs demonstrate a similar distribution. The calculated wall-shear stress distribution at 0.43 m^2 of BSA is illustrated in Figure 4, as viewed from the posterior aspect. For the Lecompte model, the range of wall-shear stress value is broader (ie, less uniform). The regions of low wall-shear stress (4-8 dynes/cm^2) and minimal wall-shear stress (<4 dynes/cm^2) are considerably large. Low and minimal wall-shear stresses are observed near the posterior portion of the bifurcation, where an abnormally low velocity gradient takes place. For the spiral model, the wall-shear stress is more uniform. The regions of low wall-shear stress are scanty, and there is no minimal wall-shear stress region at all.

Power Loss Ratio

It is evident that the power loss ratio is less for the spiral than the Lecompte model at any age (ie, various BSAs; Figure 5). The power loss ratio discrepancy between the spiral and Lecompte models increases as the BSA increases. The power loss ratio for the Lecompte model decreases from 0.25 m^2 (neonatal stage) to 0.43 m^2 (12 months of age) of BSA and increases abruptly afterward, whereas this turning point takes place at 0.45 m^2 of BSA for the spiral model. The power loss ratio decreases faster before the turning point and increases slower after the turning point for the spiral model.

Discussion

Numeric simulation has been used to obtain the flow field of 3-dimensional cavopulmonary connection and arterial bifur-

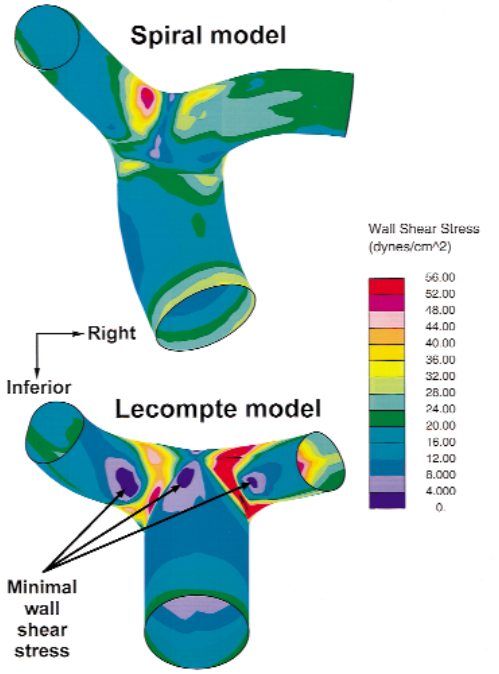

Figure 4. The wall-shear stress distribution of 2 models viewed from the posterior aspect at 0.43 m^2 of BSA. For the spiral model, the wall-shear stress is more uniform; the regions of low wall-shear stress (4-8 dynes/cm^2, *gray zone*) are scanty, and there is no minimal wall-shear stress region (<4 dynes/cm^2, *blue zone*). For the Lecompte model, the wall-shear stress distribution is less uniform. The regions of low wall-shear stress *(gray zone)* and minimal wall-shear stress *(blue zone)* are considerably large and observed near the posterior portion of the bifurcation.

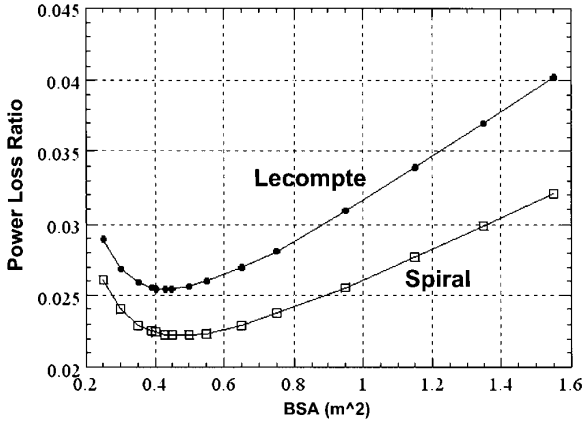

Figure 5. The calculated power loss ratio histories with respect to BSA of both models. The power loss ratio is less for the spiral than for the Lecompte model at all BSAs studied. The power loss ratio discrepancy between the spiral and Lecompte models increases as the BSA escalates. The power loss ratio of the Lecompte model drops from 0.25 m^2 (neonatal stage) to 0.43 m^2 (12 months of age) of BSA and increases abruptly afterward, whereas this turning point takes place at 0.45 m^2 (14 months of age) of BSA for the spiral model. The power loss ratio drops faster before the turning point and increases more slowly after the turning point for the spiral model than for the Lecompte model.

cations.[14-18] The total energy loss is composed of different causes in the cavopulmonary connection.[14,15] Wall-shear stress, oscillatory shear index, and spatial wall-shear stress gradient are analyzed for aortoceliac junction and carotid bifurcation.[16-18] The results suggest fluid parameters can be applied for detailed analysis of a blood vessel and its branches. None of the above-mentioned studies involves the spiral fashion of the great arteries.

Wall-shear stress distribution is of importance because local hemodynamics have been speculated to be influential on the development of stenosis, and the preferred sites of plaque are also regions of irregular wall-shear stress distribution.[19,20] It is acknowledged that low mean and oscillatory wall-shear stress tends to promote intimal thickening, whereas high shear stress inhibits the process.[20,21] The mean wall-shear stress of human arteries is approximately 15 dynes/cm^2, and stenotic plaque is prone to develop if the wall-shear stress is considerably less than this level.[21] Our results show that the Lecompte model tends to have minimal and low wall-shear regions at the posterior aspect of the PT bifurcation. It is identified that discrete stenoses frequently occur at the branches of the pulmonary arteries near the bifurcation after ASO with the Lecompte maneuver.[6,7,22] The wall-shear stress distribution of the present study indicates that minimal and low wall-shear stresses might initiate the stenosis and obstruct outflow in the pulmonary arteries because the sites of minimal and low wall-shear stresses are also the preferred locations of stenosis. The spiral model might have a better chance to remain free of plaque and stenosis.

The pressure drop and power loss ratio are smaller for the spiral than for the Lecompte model at any age. There might be no suprapulmonary stenosis after neonatal ASO with the Lecompte maneuver. As in our study, the power loss ratio is similar in both models at 0.25 m^2 of BSA, but the difference increases gradually afterward. It is widely known that suprapulmonary stenosis remains a significant problem, with a peak incidence at 9 months after conventional ASO with the Lecompte maneuver.[7] The turning point of the Lecompte model is 0.43 m^2 of BSA, which is equivalent to the age of 12 months. After this stage, the power loss ratio increases abruptly, and this might have contributed to the development of peak incidence of the suprapulmonary stenosis and the constant hazard phase that persists as long as patients are followed up.[7] The high systemic pressure of the ascending aorta may compress the neo-PT from its posterior end toward its anterior end. Insufficient dissection of the distal

CHD

pulmonary arteries was suggested to describe this flattened PT in 1988,[23] but a recent study showed that the cross section of the PT is still oval 6 to 22 months after conventional ASO with hilar dissection and the Lecompte maneuver.[10] The oval shape of the PT after the Lecompte maneuver is the result of the nonspiral arrangement. In the spiral arrangement, such as in the normal heart, there is a space for the pulmonary pathway free from compression by the aorta in systemic pressure at the aorta's left lateral portion and also at the aorta's left posterior portion. However, in the nonspiral arrangement, compression on the posterior portion of the PT from the aorta results in its oval shape. In view of the above findings, we would recommend spiral reconstruction in TGA so that the pulmonary arteries are prevented from being compressed by the posterior aorta.[11] Under natural conditions, the flow inside the pulmonary pathway is more streamlined.

It is impossible to reproduce actual physiologic conditions in this mathematic model. However, we have isolated the main variables of interest in this initial study to clarify some clinical phenomena. Subtle prototype geometry changes, such as local surface features and minor curvatures, are considered less important and would not significantly alter the flow and wall-shear stress distributions as reported.[24] Pulsation, anastomosis offset, and heterogeneous velocity profile, which could be important to the flow field, will be investigated in ongoing studies.

In conclusion, the functional superiority of the spiral model over the Lecompte model is clearly demonstrated in terms of more uniform velocity and wall-shear stress and smaller pressure drop and power loss ratio. Spiral ASO to restore the natural spiral relationship of the great arteries might be recommended in their transposition.

CHD

References

1. Kirklin JW, Blackstone EH, Tchervenkov CI, Castaneda AR. Clinical outcomes after the arterial switch operation for transposition: patient, support, procedural, and institutional risk factors. *Circulation.* 1992;86:1501-15.
2. Serraf A, Lacour-Gayet F, Bruniaux J, Touchot A, Losay J, Comas J, et al. Anatomic correction of transposition of the great arteries in neonates. *J Am Coll Cardiol.* 1993;22:193-200.
3. Shaher RM. Complete and inverted transposition of the great vessels. *Br Heart J.* 1964;26:51-66.
4. Van Mierop LHS. Transposition of the great arteries. I. Clarification or further confusion? *Am J Cardiol.* 1971;28:735-8.
5. Lecompte Y, Zannini L, Hazan E, Jarreau MM, Bex JP, Tu TV, et al. Anatomic correction of transposition of the great arteries. *J Thorac Cardiovasc Surg.* 1981;82:629-31.
6. Wernovsky G. Follow-up studies after the arterial switch operation [Letter]. *J Thorac Cardiovasc Surg.* 1998;115:481-2.
7. Williams WG, Quaegebeur JM, Kirklin JW, Blackstone EH. Outflow obstruction after the arterial switch operation: a multiinstitutional study. *J Thorac Cardiovasc Surg.* 1997;114:975-90.
8. Pasquini L, Sanders SP, Parness IAA, Colan SD, Van Praagh S, Mayer JE Jr, et al. Conal anatomy in 119 patients with D-loop transposition of the great arteries and ventricular septal defect: an echocardiographic and pathologic study. *J Am Coll Cardiol.* 1993;21:1712-21.
9. Aoki M, Forbess JM, Jonas RA, Mayer JE Jr, Castaneda AR. Result of biventricular repair for double-outlet right ventricle. *J Thorac Cardiovasc Surg.* 1994;107:338-50.
10. Massin MM, Nitsch GB, Däbritz S, Seghaye MC, Messmer BJ, von Bernuth G. Growth of pulmonary artery after arterial switch operation for simple transposition of the great arteries. *Eur J Pediatr.* 1998;157:95-100.
11. Chiu IS, Wu SJ, Chen MR, Lee ML, Wu MH, Wang JK, et al. Modified arterial switch operation by spiral reconstruction of the great arteries in transposition. *Ann Thorac Surg.* 2000;69:1887-92.
12. Rowlatt UF, Rimoldi HJA, Lev M. The quantitative anatomy of the normal child's heart. *Pediatr Clin North Am.* 1963;10:499-588.
13. STAR-CD Manual, version 3.05. London: Computational Fluid Dynamics Corp, Ltd; 1998.
14. de Leval MR, Dubini G, Migliavacca F, Jalali H, Camporini G, Redington A, et al. Use of computational fluid dynamics in the design of surgical procedures: application to the study of competitive flows in cavopulmonary connections. *J Thorac Cardiovasc Surg.* 1996;111:502-13.
15. Van Haesdonck JM, Mertens L, Sizaire R, Montas G, Purnode B, Daenen W, et al. Comparison by computerized numeric modeling of energy losses in different Fontan connections. *Circulation.* 1995;92(Suppl II):II-322-26.
16. Buchanan JR Jr, Kleinstreuer C, Truskey GA, Lei M. Relation between non-uniform hemodynamics and sites of altered permeability and lesion growth at the rabbit aorto-celiac junction. *Atherosclerosis.* 1999;143:27-40.
17. Delfino A, Stergiopulos N, Moore JE Jr, Meister JJ. Residual strain effects on the stress field in a thick wall finite element model of the human carotid bifurcation. *J Biomech.* 1997;30:777-86.
18. Milner JS, Moore JA, Rutt BK, Steinman DA. Hemodynamics of human carotid artery bifurcations: computational studies with models reconstructed from magnetic resonance imaging of normal subjects. *J Vasc Surg.* 1998;27:143-56.
19. Fry DL. Responses of the arterial wall to certain physical factors: In: Porter R, Knight J, editors. Atherogenesis: initiating factors. Amsterdam: Associated Scientific Publishers; 1973. p. 93-125.
20. Caro CG, Fitz-Gerald JM, Schroter RC. Atheroma and arterial wall shear observations correlation and proposal of a shear dependent mass transfer mechanism for atherogenesis. *Proc R Soc Lond B Biol Sci.* 1971;177:109-59.
21. Giddens DP, Zarins CK, Glagov S. Response of arteries to near-wall fluid dynamic behavior. *Appl Mech Rev.* 1990;43:S98-102.
22. Smoot LB, Wernovsky G, Mayer JE Jr, Hanley FL, Keane JF. Results of balloon angioplasty in patients with right ventricular outflow tract obstruction following the arterial switch operation [abstract]. *Circulation.* 1992;86(Suppl):I-42A.
23. Wernovsky G, Hougen TJ, Walsh EP, Sholler GF, Colan SD, Sanders SP, et al. Midterm results after the arterial switch operation for transposition of the great arteries with intact ventricular septum: clinical, hemodynamic, echocardiographic, and electrophysiologic data. *Circulation.* 1988;77:1333-44.
24. Moore JA, Steinman DA, Prakash S, Johnston KW, Ethier CR. A numerical study of blood flow patterns in anatomically realistic and simplified end-to-side anastomosis. *J Biomech Eng.* 1999;121:265-72.